Breaking down the tropospheric circulation response by forcing

Paul W. Staten
Department of Atmospheric Sciences
135 S 1460 E, Rm. 819 (WBB)
Salt Lake City, UT 84112
University of Utah
Tel: +1-801-581-6136
Fax: +1-801-581-4362
paul.staten@utah.edu

Jonathan J. Rutz
Department of Atmospheric Sciences
135 S 1460 E, Rm. 819 (WBB)
Salt Lake City, UT 84112
University of Utah
Tel: +1-801-585-0040
Fax: +1-801-581-4362
jon.rutz@utah.edu

Thomas Reichler
Department of Atmospheric Sciences
135 S 1460 E, Rm. 819 (WBB)
Salt Lake City, UT 84112
University of Utah
Tel: +1-801-585-0040
Fax: +1-801-581-4362
thomas.reichler@utah.edu

Jian Lu
IGES / COLA
4041 Powder Mill Road, Suite 302
Calverton, MD 20705-3106
Center for Ocean-Land-Atmosphere Studies
Tel: +1-301-595-7000

UU IR Author Manuscript

Fax: +1-301-595-9793

jianlu@cola.iges.org

This study describes simulated changes in the general circulation during the twentieth and twenty-first centuries due to a number of individual direct radiative forcings and warming sea surface temperatures, by examining very long time-slice simulations created with an enhanced version of the Geophysical Fluid Dynamics Laboratories Atmospheric Model AM 2.1. We examine the effects of changing stratospheric ozone, greenhouse gas concentrations, and sea surface temperatures individually and in combination over both hemispheres. Data reveal robust poleward shifts in zonal mean circulation features in present-day simulations compared to a pre-industrial control, and in future simulations compared to present-day. We document the seasonality and significance of these shifts, and find that the combined response is well approximated by the sum of the individual responses. In contrast with other recent studies, we find that circulation shifts due to changing sea surface temperatures – not ozone depletion or recovery – dominate the combined southern hemisphere response during all seasons, and accordingly project that the southern hemisphere jet will continue to shift poleward during the twenty-first century.

Global climate modeling; General circulation; Stratosphere/troposphere interactions

20C3M: twentieth century AR4 simulation; AM: annular mode; AM2.1: Atmospheric Model v. 2.1; AR4: fourth assessment; CAM3: Community Atmosphere Model version 3; CCM: coupled chemistry climate models; CM2.1: climate model version 2.1; CMAM: Canadian Middle Atmosphere Model; CMIP3: Coupled Model Intercomparison Project; DJF: December, January, and February; DP09: Deser and Phillips (2009); ERA-40: European Centre for Medium-Range Weather Forecasts 40 Year Re-analysis Project; GFDL: Geophysical Fluid Dynamics Laboratory; IPCC: Intergovernmental Panel on Climate Change; ITCZ: intertropical convergence zone; JJA: June, July, and August; K11: Kang et al. (2011); NAM: northern annular mode; NCAR: National Center for Atmospheric Research; NH: northern hemisphere; P10: Polvani (2010); P-E: precipitation – evaporation; SAM: southern annular mode; SH: southern hemisphere; SST: sea surface temperature

1. Introduction

The observed global mean temperature increase during the last century is a symptom of a more fundamental change in the earth climate system: the changing distribution of radiative heating and cooling, and the resulting shifts in the general circulation of the atmosphere. One theme in past studies has been the poleward expansion of important circulation features. These circulation shifts, in concert with the changes in atmospheric thermodynamical structure, are of particular concern because they have the potential to produce profound changes in surface climate and precipitation patterns.

Observations and simulations depict a poleward shift in many global circulation patterns during the past century. Estimates of tropical widening, beginning with Rosenlof (2002), range from 0.3

UU IR Author Manuscript

to 3.1° latitude per decade, depending on the season, hemisphere, and dataset (Seidel et al. 2008; Reichler 2009; Hu et al. 2011). Understanding the cause of these changes has proven difficult, as model simulations seem to underestimate observed tropical widening trends. The cause of this discrepancy is an outstanding issue (Johanson and Fu 2009).

Studies have also shown a poleward shift in extratropical circulation features in both hemispheres, broadly consistent with a shift towards more positive annular modes (hereafter AMs; Kushner et al. 2001; 2009). As with tropical width, general circulation models seem to underestimate the observed change in the northern annular mode (NAM) index (Miller et al. 2006).

Models quite accurately reproduce observed changes in the southern annular mode (SAM), with widening being attributed to ozone depletion and, to a lesser degree, greenhouse gas emissions (Arblaster and Meehl 2006; Perlwitz et al. 2008). Comparing coupled chemistry climate models (CCMs) with simulations from the third phase of the Coupled Model Intercomparison Project (CMIP3), Son et al. (2008; 2009a; 2009b) found that future ozone recovery may cancel out or even reverse the poleward tendency of the midlatitude jet due to greenhouse gas increases and sea surface temperature (SST) warming. These studies include many different models of varying quality, which may make it difficult to cleanly separate the effects of individual forcings from the effects of model differences.

To alleviate this difficulty, Deser and Phillips (2009; hereafter referred to as DP09) examined ten-member ensembles of 1950-2000 transient climate simulations using the National Center for Atmospheric Research (NCAR) Community Atmosphere Model version 3 (CAM3) to compare the direct effects of radiative forcings and the indirect effect of changing SSTs on the general circulation. Their study emphasized the role that direct radiative forcings played in shifting extratropical precipitation patterns, but did not distinguish between the effects of greenhouse gases or ozone depletion. In addition, DP09 prescribed observed SSTs, introducing inconsistencies and sensitivity to natural slow oscillations in SSTs (e.g. the Pacific decadal oscillation and El Niño Southern Oscillation).

In order to analyze the effects of ozone depletion, Polvani et al. (2010; hereafter P10) also examined CAM3 time-slice simulations. P10 emphasized the role of ozone depletion during southern hemisphere (SH) summer (DJF), predicting an equatorward shift of the midlatitude jet during the twenty-first century due to the expected recovery of stratospheric ozone. They also

noted an approximate linearity of the climate response to ozone and greenhouse gas forcings. However, P10 investigated 50-year time-slice simulations; longer simulations would be desirable for filtering natural climate variability. In addition, P10 did not separate the direct radiative effects of greenhouse gases from the indirect effect of SSTs.

Kang et al. (2011; hereafter K11) analyzed time-slice simulations from both CAM3 and the Canadian Middle Atmosphere Model (CMAM), and also predicted an equatorward SH jet shift during DJF. K11 improved on previous studies by performing a coupled simulation, as well as uncoupled simulations utilizing both observed SSTs and SSTs from the coupled simulation. However, they did not vary greenhouse gas concentrations, and thus could not separate the effects of greenhouse gases from the effects of ozone depletion or changing SSTs.

Perlwitz et al. (2008) and McLandress et al. (2011) likewise examined CCM data and reiterated the importance of ozone depletion in twentieth century climate change over the SH. These studies predicted that the SH tropospheric circulation response to ozone recovery and increased greenhouse gases will roughly cancel each other out during DJF. However, Perlwitz et al. (2008) used SSTs from observations or other models, while McLandress et al. (2011) exclusively performed coupled simulations. The former may thus have SSTs that are inconsistent with the model, while the latter cannot explicitly separate the direct radiative effects of the different forcings from the indirect effects of the resulting SST changes.

The present study is concerned with understanding how ozone depletion and recovery, greenhouse gas increases, and SST changes each contribute to shifts observed during the 20th century and to shifts expected during the 21st century. The outcome of this work may help to shed light on why models often underestimate tropical and northern hemisphere (NH) circulation shifts, as quantifying the response to individual forcings is a step towards understanding the overall response. It will also aid in better understanding the mechanisms behind such change by isolating interfering, and at times competing, effects.

Of the studies described above, only Perlwitz et al. (2008) compare ozone depletion, greenhouse gas increases, and SST warming each in isolation. We likewise examine each forcing separately and in combination, using 500-year-long time-slice simulations produced by an enhanced version of the Geophysical Fluid Dynamics Laboratory (GFDL) Atmospheric Model v. 2.1 (AM2.1; Anderson et al. 2004)). We specify pre-industrial, present day, and future ozone levels, greenhouse gas concentrations, and SSTs. Also in contrast to most of the studies described above

(K11 being the only exception), we take decadally averaged SSTs from a companion coupled model – not from observations – in order to filter out interannual SST variability and to apply model-consistent SST patterns.

Section 2 documents our experimental setup and methods. Section 3 details the circulation response to various forcings by hemisphere and season. Section 4 contains a brief summary, and discusses the implications of our results in light of recent literature.

2. Data and methods

Here we describe the model setup used in this study. We then detail the prescribed forcings to be investigated. As we are mainly interested in zonal mean circulation changes, we finish this section by defining the circulation indicators used in this study.

Following Fletcher et al. (2009), we use an enhanced version of AM2.1, with 48 levels in the vertical, rather than the standard 24. This is the same model as that used in Austin et al. (2007), but without interactive chemistry. Most of the additional layers are above 100 hPa, producing a well-resolved upper troposphere and lower stratosphere. Horizontal grid resolution is approximately 2° latitude by 2.5° longitude.

We prescribe well-mixed greenhouse gases at their historical, present-day, and projected levels, with projected levels of CO_2, CH_4, and N_2O taken from the Intergovernmental Panel on Climate Change (IPCC) A1B scenario. We take zonal mean ozone data from the Randel and Wu (2007) dataset, with monthly mean values taken from pre-1980 years for the pre-industrial and future states, and from the year 2000 for the present-day, depleted ozone state (see Figure 1a). The Randel and Wu (2007) dataset draws from similar data as the SPARC ozone database (Cionni et al. 2011), which is used in several of the above-mentioned studies.

[Figure 1 about here]

The ozone depletion prescribed in our study is dominated by the SH ozone hole, with the strongest depletion in September-October-November. The NH also experiences spring-time depletion, albeit much weaker. In the tropics we see some year-round increase. We refer the reader to Randel and Wu (2007) for a more complete description of the changes in this dataset.

We derive SSTs from the fully coupled Climate Model v2.1 (CM2.1; Delworth et al. 2006), the coupled companion model to AM2.1. Prescribing SSTs from the coupled model ensures that SSTs are mostly consistent with the circulation of the AM2.1 model. In order to reduce the

effects of natural SST variability, such as the El Niño Southern Oscillation, we calculate multi-year average SSTs for each month. Pre-industrial SSTs are taken from 10 years of data from the pre-industrial control run (PIcntrl) prepared for the IPCC fourth assessment report (AR4). Present-day and future SSTs are derived from the twentieth century (20C3M) and A1B future scenarios, both also performed for the IPCC AR4, with present-day SSTs being averaged over 1997-2006, year-2050 SSTs being averaged over 2045-2055, and year-2100 SSTs being averaged over 2081-2100.

The changes in SSTs shown in Figure 1 include the temperature of regions formerly covered with sea ice. From 1870 to 2000 (Figure 1b), and from 2000 to 2050 (Figure 1c), much of this sea ice melts, increasing the temperature in the associated grid cells, and creating the impression of strong SST increases. This impression is valid, as this melting leads to strong, anomalous surface heat flux, and plays an important part in the well known poleward amplification of warming. We also note differences in the structure and seasonality of present day and future SST changes. These differences in turn affect our projections of future climate. The SST changes from 2000 to 2100 (not shown) closely resemble the changes from 2000 to 2050, only stronger.

Using prescribed SSTs has the important benefit of allowing us to distinguish between the direct effect of radiative forcing due to greenhouse gas increases and ozone depletion, and the indirect effect (see DP09) of the SST response to the combined forcings. What we term the direct effect is the atmospheric temperature and circulation response to radiative forcings within the atmosphere itself, without allowing SSTs to respond. The indirect effect is the response of the atmosphere to just the changing SSTs, which are themselves a response to all the known forcings in a coupled model. This approach is useful for studying the mechanisms behind circulation shifts, as a given radiative forcing may cause a circulation shift via one set of mechanisms, while the SST response to that forcing may alter the general circulation via some other mechanisms. Thus the circulation change produced when both the radiative forcings and SST responses are included will be formed through a combination of mechanisms.

As aerosols in AM2.1 act largely by cooling the ocean surface (Ming and Ramaswamy 2009), the direct radiative effect of aerosols in AM2, while holding SSTs at their unperturbed state (not shown in this study) is quite small. For this reason, we prescribe aerosols at their pre-industrial levels for all our simulations. This illustrates one drawback to using prescribed, rather than coupled, SSTs. While we can examine separately the radiative effects of ozone and greenhouse

gases, we cannot prescribe the SST response to just one forcing or another without running the fully coupled model. Thus, the SST in this study are in response to the complete set of all known forcings during the time period over which we calculate the average SSTs, i.e., radiatively active trace gases, aerosols, and land use changes.

We choose combinations of past, present and future prescribed forcings to perform three sets of time-slice simulations in this study. Our '2000' simulations examine the individual and combined effects of year-2000 forcings, compared to a year-1870 pre-industrial control. Simulations labeled '2050' and '2100' examine the effects of year-2050 and year-2100 forcings, respectively, compared to a year-2000 control (see Table 1). Simulations in which only greenhouse gases are perturbed from their control levels are labeled, simply, 'CO_2.' Perturbed ozone simulations are labeled 'O_3', and perturbed SST simulations are labeled 'SST.' Simulations with all three forcings perturbed simultaneously are labeled 'all'. The simulations in our study are all at least 500 years long, and represent a subset of the simulations performed at the University of Utah using the AM2.1 model.

[Table 1 about here]

The '2000' and '2050' simulations are performed precisely as described—with forcings held at their respective control levels except for those labeled. However, we have not yet performed mixed present-day and year-2100 simulations. To reduce computational cost, we approximate these differences using an existing set of simulations, and compare specific present-day and year-2100 forcings, with the other forcings held at their pre-industrial values. For example, the '2100 SST' simulations are examined by using year-2000 SSTs for the control and year-2100 SSTs for the experiment, but 'CO_2' and 'O_3' forcings are held at their 1870 levels in both simulations. This approach is valid inasmuch as the response to external forcings is linear; this assumption turns out to be reasonable, as we will illustrate using the '2000' and '2050' simulations.

A considerable portion of this study deals with changes in zonal mean climate features. Here we describe how these zonal mean features are calculated. We isolate zonal mean temperature, zonal wind, sea level pressure, precipitation, surface evaporation, and the mass meridional stream function (Ψ) data. We then perform a cubic spline interpolation after Hu et al. (2011), resampling to a 0.2° latitude grid, and smooth the data using a Gaussian kernel with a 7° latitude standard-deviation. This smoothing is useful in reducing the sensitivity of the threshold indicators to noise

in the data. We also find it desirable to obtain an integrated measure of large-scale circulation change, rather than localized changes in cell structure.

Once our data are interpolated and smoothed in latitude, we calculate the poleward Hadley cell boundaries (hereafter Hadley cell edges) as the first zero crossings of $\Psi_{500\,hPa}$ poleward of the intertropical convergence zone (hereafter ITCZ), after Lu et al. (2007). The first zero crossing poleward of ±50° in either hemisphere is denoted the Ferrel cell edge. To calculate the surface zonal wind zero crossing poleward of the surface easterlies, we first calculate the latitude of maximum surface zonal winds equatorward of ±70° latitude, and then take the first surface wind zero crossing equatorward of this maximum.

We define the precipitation – evaporation (P-E) zero crossing (P-E=0) as the first zero crossing of the P-E field poleward of the latitude of minimum P-E, after K11. We calculate the latitude of maximum precipitation over ±30°-70° latitude.

Annular modes are calculated from zonal mean sea level pressure data poleward of ±20° latitude (Baldwin and Thompson 2009). For consistency, we use the present-day time-slice simulation to produce a loading pattern. The pressure anomaly for each dataset with respect to the control time-slice simulation is then projected onto this pattern to produce an AM time series for each dataset.

Changes in zonal mean quantities presented in this study, including temperature, wind, and the indicators described above are presented with measures of significance. We calculate the significance from decadally averaged raw data, using a student's t-test with unequal sample sizes and unequal variances. It should be kept in mind, however, that the zonal mean indicators described above and their associated confidence intervals are calculated from the latitudinally smoothed fields. The calculations based on unsmoothed fields occasionally produce extreme values for a given month and forcing, with accompanying low confidences in those cases. In general, however, the magnitudes and seasonalities of the different indicators are fairly insensitive to the degree of latitudinal smoothing.

The length of our time-slice experiments (at least 500 years) allows us to effectively suppress the effects of sampling uncertainty due to natural variability. Our data are smooth, and our signals usually highly statistically significant. In addition, we use 10-year averaged model-simulated SSTs to reduce the effects of SST variations.

3. Results

3.1 The zonal mean response

Before examining the specific changes in the circulation, we take a holistic view of temperature and zonal wind changes during the summer and winter seasons. Figure 2 shows the temperature responses due to individual and combined forcings in '2000' and '2050' during December-January-February (DJF). Figure 3 shows the corresponding zonal wind responses. The June-July-August (JJA) temperature and zonal wind responses are shown in the supplementary material in Figures S1 and S2, respectively, and the '2100' temperature and zonal wind responses for DJF are both represented in Figure S3. We note that the '2100' responses are similar to those in '2050', albeit generally more pronounced.

[Figure 2 about here]

Ozone depletion ('O_3'), as expected, acts mainly to cool the stratosphere, particularly over the summer hemisphere lower stratosphere (Figures 2a, S1a). This effect is strongest over the SH, with peak cooling of over 2°C at 100 hPa, poleward of 80 °S. Ozone recovery (Figures 2b, S1b, S3a) produces nearly equal and opposite temperature changes. The effect of ozone depletion or recovery on tropospheric temperatures is small and mostly insignificant at the 5% level. However, cooling extends near the surface over Antarctica, consistent with Gillett et al. (2003). Increasing greenhouse gas concentrations ('CO_2') contribute to stratospheric cooling of at least 1°C above 60 hPa during both DJF and JJA, intensifying with height at least up to 10 hPa (Figures 2, S1, S3). The tropospheric temperature response is small, but still significant in spite of using fixed control SSTs. The seasonal change in the temperature response to greenhouse gas increases is much smaller than that due to ozone depletion or recovery, since greenhouse gas concentrations vary little over the course of the year compared to ozone concentrations.

In contrast to changing ozone and greenhouse gas concentrations, SST increases ('SST') significantly warm the troposphere, with warming often exceeding 1°C in '2000' and 2°C in the future scenarios. This warming is strongest during the respective winter of each hemisphere. In contrast, the stratosphere cools year-round in the vicinity of the tropopause and over the tropics. This pattern of warming and cooling is likely associated with a rise in tropopause heights, and is an expected consequence of SST warming (Lu et al. 2010).

The combined forcings ('all') act constructively over the past century (Figure 2g, S1g), cooling the SH lower stratosphere over 4 °C and warming the tropical troposphere over 2 °C during DJF. During JJA, responses are weaker but the additive effect of the forcings is still clearly evident. In future simulations (Figure 2h, S1h, S3g), greenhouse gas increases and SST warming compete with ozone recovery, with net warming over the SH lower stratosphere due to ozone recovery in 2050 changing to slight but significant cooling by 2100 (Figure S3g).

Shifting our focus now to the zonal mean wind response (see Figures 3, S2, S3), we note that the stratospheric response can be characterized to a first order as being in thermal wind balance with the stratospheric temperature response. Ozone depletion alone strengthens SH stratospheric westerlies by as much as ~2 ms^{-1} over the SH, while it weakens NH stratospheric westerlies by ~1 ms^{-1} during DJF, with a weakly opposite response during JJA. In contrast to the stratospheric response, the tropospheric response to ozone is small except for a meridional dipole near the SH jet, with winds along the poleward flank of the SH jet increasing or decreasing by about 1 ms^{-1} at the surface, with larger changes aloft. Ozone recovery again has the opposite effect. The dipole about the tropospheric jet suggests a dynamical downward influence of the stratosphere on the troposphere, reminiscent of the results of Polvani and Kushner (2002).

[Figure 3 about here]

Greenhouse gas increases induce year-round easterly anomalies in the tropics (less than 0.5 ms^{-1}), and westerly anomalies in southern high latitudes (up to 1 ms^{-1}), with a similar dipole structure about the SH tropospheric midlatitude jet as from ozone depletion during DJF, again extending down to the surface. NH changes include a weak, but at times significant, deceleration along the poleward flank of the midlatitude jet during DJF, which changes to an acceleration during JJA.

SSTs exhibit a strong control over tropospheric circulation, as they largely dictate the temperature and humidity structure of the entire troposphere. SST warming produces stronger dipole wind anomalies about the midlatitude jet than that produced by either greenhouse gas increases or ozone changes alone. These dipoles are stronger over the SH than for the NH during both DJF and JJA. In '2050' and '2100' during DJF, we see a localized strengthening of winds about the SH tropical tropopause.

The model responses to the combined forcings ('all') very nearly match the linear combination of the responses to individual forcings (not shown), with ozone depletion, greenhouse gas

increases, and SST warming all acting to shift the tropospheric jets poleward for the '2000' climate simulation. In future simulations, greenhouse gas increases and SST warming act together to overcome the response to ozone recovery, still shifting the tropospheric jets poleward. The clear similarities between the 'SST' and 'all' figures reiterate the importance of the indirect SST effect in shaping the overall circulation response to external forcings.

In general, SH winds respond more strongly than NH winds to any type of forcing. The weak SH wind response in '2050 all' (Figure 3h) appears to be an exception at first glance. Upon closer examination, however, the weak SH response to the combined forcings turns out to be a cancellation of (1) a strong positive response to SST warming (Figure 3f), and (2) a strong negative response to ozone recovery (Figure 3b). Thus the net SH response is weak.

The '2000' DJF temperature and zonal wind responses to the combined forcings agree very well with the linear temperature and wind changes during 1979-2000 in the European Centre for Medium-Range Weather Forecasts 40 Year Re-analysis Project (ERA-40; not shown). ERA-40 data are generally noisier, and include some localized cooling in the tropical mid-troposphere, as well as a deceleration of the surface easterlies in the deep tropics. More importantly, the SH lower stratosphere exhibits a linear cooling trend about 50% stronger than our '2000 all' simulated response. If the observed trend is to be taken at face value, then this suggests that either our model's thermal response to ozone depletion is too small, or that our prescribed ozone depletion is too weak. Our simulated tropospheric wind response, on the other hand, is quite realistic.

3.2 The seasonality of selected circulation features

Now that we have presented a broad picture of the changes in zonal mean temperature and wind patterns, we focus on specific indicators of the tropospheric circulation and the fine scale structure of their seasonal cycles. In the previous section, dipoles in zonal wind allowed us to qualitatively infer latitudinal shifts in circulation features. Here we quantify such shifts, beginning with the Hadley cell edge. The following sections will refer extensively to Figures 4 and 5. The precise descriptions of the indicators discussed are explained in Section 2. The time periods and forcings are listed in Table 1, and annual mean changes for each experiment and forcing are quantified in Table 2.

During the past century, the Hadley cell edges shift slightly poleward (less than 0.3°) under the influence of radiative forcings alone, but substantially (up to 1°) under the influence of warming SSTs. Shifts are largest during the summer of each hemisphere, in agreement with the observational study by Hu and Fu (2007), amplifying the seasonal swings in Hadley cell extent. Ozone depletion produces its largest shifts during austral spring and summer, and smaller, mostly insignificant changes during the rest of the year, owing to the seasonally varying nature of ozone forcing.

[Figure 4 about here]

During the 21st century (see Figure 4b, c), the effects of ozone recovery (blue curve) over the SH neatly oppose those from ozone depletion. Recovery-induced changes over the NH are small and almost nowhere significant, even in the annual mean. By '2100', greenhouse gas increases (red curve) shift the Hadley cell edges poleward significantly year-round over both hemispheres (0.7 to 0.3° in the annual mean).

SST warming (orange curve) shifts the Hadley cell edges significantly during most seasons, in all three time periods studied. Annual mean poleward Hadley cell edge shifts due to SST warming (Table 2) span nearly an order of magnitude, from less than 0.1° during the 20th century to 0.7° during the 21st century. This dominant SST impact holds for all indicators analyzed in this study.

During '2000', in addition to the expected summertime shift, SST warming also strongly affects the Hadley cell edges during May in both hemispheres, producing over 1° widening of the tropics. In contrast, future changes during May over the NH are close to zero, and are strongest instead during the fall. The effects of future SST warming on the SH Hadley cell are overall relatively weak in '2050', only becoming strong year-round by '2100'. We note that the structure and seasonality of the SST forcing used to drive the '2000' and '2050' simulation sets also differ (see Figure 1b, c), which may help to explain some of the differences.

The linear sum of the effects of the individual forcings (gray) is very similar to the effect of the combined forcings (black), even in many minor details. It is significant that the linear sum for '2100' approximates the combined response as well as it does, considering that the linear sum for the '2100' includes (1) errors of the sum, as with the '2050' and '2000' cases, and (2) errors of the substitution, or errors from using purely forced experiments to approximate mixed forcing experiments (see Section 2 and Table 1). The match between the '2100' linear sum and

UU IR Author Manuscript

combined-forcings run validates the assumption of linearity, as well as our choice of substitution. That said, we see departures from linearity during JJA in the future scenarios (Figure 4b, c), and while we do not test the significance of these differences, they appear to be real and systematic. In summary, we see mostly poleward shifts in the Hadley cell boundary, with strong seasonalities. Over the past century, this seasonal cycle peaks in the summertime over both hemispheres, although the largest overall widening occurs in May due to the phase difference of the NH and SH shifts. This detail in seasonality is a slight departure from that in observations (Hu and Fu 2007), in which similar shifts during the summer and fall of each hemisphere produce fairly consistent year-round tropical widening. Future simulations produce more year-round widening, and a different seasonality. Shifts over the NH become stronger than shifts over the SH, even during seasons with no cancelling effect from ozone depletion over the SH; changes in the SST response are mostly responsible for the strong NH shift. The reasons for this change in seasonality from '2000' to '2050' and '2100' are unclear. We suspect that non-linear behavior, as well as changes in the structure of the driving SSTs and sea ice, might play a role; such structural changes may include the direct effect of aerosols on SSTs. In general, the SST effect dominates shifts in the Hadley cell, producing a response similar to that of the combined forcings, which in turn very closely resembles the linear sum of the individual responses.
The descending branches of the Hadley cell are roughly co-located with the subtropical high pressure cells and consequently with zero crossings of the zonal wind at the surface. Here we use the surface wind zero crossing (hereafter U=0; see Figure 4, second row) to take another look at tropical widening. Overall, latitudinal shifts in the Hadley cell and U=0 are similar in magnitude, but differences exist in the details and seasonality. For example, shifts occur earlier in the year over the NH than for the Hadley cell edge. This NH-SH phase difference produces tropical widening in most seasons during '2000'. By '2100', strong NH changes contribute to widening of as much as 2°.

We now shift our focus to the Ferrel cell, motivated by its strong ties to surface hydrology features and by the strong effect of ozone depletion on mid- and high-latitude winds (see Figure 3). Not surprisingly, the Ferrel cell edge shifts strongly due to ozone depletion and recovery during SH Spring (Figure 4, third row; note the differing axes). In '2000' and '2050', ozone changes at times shift the Ferrel cell more than either greenhouse gas increases or SST warming.

But in our simulations, the combined effect of the latter two forcings consistently and strongly outweighs the effect of ozone recovery in '2050' and '2100', in contrast to DP09.

Work by Staten et al. (2010) suggests that poleward circulation features generally shift more than their equatorward counterparts. In the present study, we see again that the Ferrel cell edge shifts more strongly (at nearly 6°) than the Hadley cell edge (at about 1.5°), implying a widening of the Ferrel cell. This widening is substantial in both hemispheres throughout most of the year, except over the SH during JJA, giving rise to a seasonality distinct from that of the Hadley cell.

Up to this point we have presented our results in an equator-to-pole fashion. We now turn our attention to the AMs (Figure 4, bottom row), which can be seen as an integrated measure of the circulation over each hemisphere (poleward of ±20°). Here we examine how changes in the mean state project onto the AM patterns calculated from present-day climate. Positive values here reflect a decrease in sea level pressure over the poles and a poleward shift of midlatitude westerlies, similar to what we would expect with a poleward-shifting Ferrel cell. It is interesting to note, therefore, that the seasonalities of the above described extratropical circulation changes over the NH differ markedly from that of the NAM. The NAM response is very muted in summer but strong during early winter and spring, particularly in '2050' and '2100'. In contrast, the SAM response is strongest during SH summer as with the Ferrel cell edge response. The strong responses over the NH are roughly coincident with the active seasons of the NAM, when coupling between the stratosphere and the troposphere is expected to be strongest (Thompson and Wallace 2000). It is also noteworthy that, as with the other circulation indicators, the seasonality of the AM response to SST warming changes sharply between the '2000' scenario and the '2050' and '2100' scenarios.

3.3 The seasonality of selected hydrological features

Our interest in the circulation indicators described above ultimately stems from their importance to surface climate, particularly hydrology. While these circulation features described above have fairly similar seasonalities, the hydrological indicators in this study (see Figure 5) exhibit a seasonality that is quite distinct from that of our dynamical indicators. This is consistent with Hu et al. (2011), who also find differing seasonalities when comparing hyrdological versus dynamical or radiative indicators of tropical width.

[Figure 5 about here]

Here we examine the zero crossing of precipitation minus evaporation (P-E=0; Figure 5, top row) in the tropics, noting its link to the subsiding branch of the Hadley cell. Not surprisingly, the seasonality of P-E=0 more closely resembles that of U=0 at the surface, rather than the mid-tropospheric Hadley cell edge at 500 hPa. We see a similarity in the seasonality of P-E=0 to the observed subtropical precipitation minimum trends described in Hu et al. (2011), with a NH peak during March-April-May, and a SH peak during DJF, but little agreement with the observed seasonality of the subtropical dry zone trends presented in Zhou et al. (2011).

SST warming produces poleward P-E=0 shifts in '2000' with a seasonality similar to that for U=0 (Figure 4d), but in '2050' and '2050' it produces poleward P-E=0 shifts year-round, with a pronounced 1.5° latitude peak in July over the NH; the ~0.7° shift over the SH is substantial as well. Again, SST warming explains the shifts in the combined response to a large extent; the effects of direct radiative forcings alone are similar to those described for the dynamical indicators above, and are particularly weak for P-E=0.

Moving our attention once more to the extratropics, we see that shifts in the midlatitude precipitation maxima (Figure 5, bottom row), which are indicative of shifts in the location of stormtracks, and are thus reminiscent of shifts of the edge of the Ferrel cell (Figure 4, third row). Over the NH, warming SSTs shift the Ferrel cell edge more than the precipitation maximum, while over the SH, warming SSTs shift the SH precipitation maximum more than the SH Ferrel cell edge.

4. Summary and discussion

We perform time-slice simulations using the GFDL AM2.1 model to diagnose anthropogenically-induced shifts in the general circulation during the twentieth and twenty-first centuries. Forcings over the past century have produced statistically significant poleward shifts in upper level circulation patterns, as well as surface circulation and hydrology patterns. Estimates of tropical widening are within the range of previous modeling studies. Our simulations suggest that SST warming, and its dominant impact on the thermal structure and moisture distribution in the troposphere, play a crucial role in the response of the general circulation and global hydrological cycle to anthropogenic forcings. Perhaps the most important outcome of this study is our projection that poleward shifts over the coming century will

continue over both hemispheres, and will remain significant, in spite of the competing effect of ozone recovery.

Annual mean tropical widening estimates in our study from all forcings combined are mostly below 1° latitude over the past century. Assuming most of this widening occurred during the last 25 years, this gives us a rate of ~1° per 25 years, or 0.4° per decade. This is small compared to the 2.0-4.8° per decade widening seen in observational studies reviewed by Seidel et al. (2008), and at the bottom end of the 0.3-3.0° per decade range of observational estimates listed in Reichler (2009). However, the changes are typical for the model-derived estimates discussed in Reichler (2009). Our study is unique in its use of very long time-slice simulations, all but eliminating natural variability. Our study validates the results of other modeling studies, in that our circulation shifts can be attributed with high confidence to external forcings. We conclude that the more extreme poleward trends seen in observational datasets are probably unrealistic, and largely a result of natural variability and observational sampling uncertainty.

Ferrel cell edge shifts are considerably larger than the tropical shifts in this study. While the Hadley cell widened by about 0.8° in '2000' in response to the combined forcings, the combined poleward shifts of the NH and SH Ferrel cell edges amounted to 2.5° latitude. The Hadley cell is expected to widen by an additional 1.5° in the coming century, while the combined Ferrel cell edge shifts are expected to amount to an additional 4.5°. The strong shift of the Ferrel cell edge relative to that of the Hadley cell is reminiscent of a similar pattern noted by Kang and Polvani (2010) on interannual timescales. Some of the relationships between the shifts of different circulation features are discussed in Staten et al. (2010), and are the subject of ongoing research. Preliminary results suggest that, in general, poleward circulation features shift more strongly than equatorward features. This implies (and may be parsimoniously explained by) a widening of the Ferrel cell, reminiscent of the pattern seen in Kidston and Vallis (2010) when studying climatological eddy-driven jet position and width.

In agreement with DP09, our data reveal that the effects of individual forcings on the circulation are nearly additive. We use this result to estimate '2100 SST' and '2100 CO_2' changes, as described in Section 2. The linear sum of the '2100' purely-forced changes approximates the '2100 all' changes quite well, validating this approach. Exceptions to linearity in '2050' and '2100' are strongest in general during NH summer, while in the '2000' comparisons, we see

more departures from linearity during SH summer. The consistency of these departures between experiments suggests that they are realistic.

The circulation shifts seen in this study are also reflected by changes in the AMs. The seasonality of the change in the SAM is roughly in line with that of other circulation features, while the seasonality of the change in the NAM bears little semblance to the seasonality of the Hadley or Ferrel cell edge shifts. The mismatch in the seasonality between the NAM and other circulation features illustrates that caution is needed when using AMs to examine mean changes in circulation. An increase in the AM does not clearly distinguish between changes in the structure of the circulation (e.g. the location of the midlatitude jet) and the intensity of the circulation (e.g. the strength of the jet).

In contrast with several recent studies (Deser and Phillips 2009; Polvani et al. 2011; Polvani et al. 2010; Son et al. 2010), we project that the poleward shifts in SH circulation features observed over the past century will continue throughout the next century, and remain significant in spite of ozone recovery. Our model response may be described as a combination of (1) a relatively strong indirect SST response, and (2) a relatively weak direct radiative response to changing ozone concentrations. In what follows, we contrast our responses to those from previous studies, and discuss possible reasons for the differences in these two responses.

Figure 6 shows in greater detail the sensitivity in mean DJF precipitation in response to the various forcings. This can be compared to Figure 12 in P10, to Figure 11 in DP09, and to Figure 2 in K11. All three of these other studies use CAM3, although K11 also take data from the CMAM model. DP09 examine ensembles of 50-year transient simulations, while P10 and K11 perform 50-yr time-slice simulations. Despite methodological differences between these other studies, all three depict an extratropical precipitation change due to ozone depletion or radiative forcings using CAM3 that is generally stronger than we show here due to 'O_3' or 'CO_2' using AM2.1 (Figure 6, first and second rows, respectively). On the other hand, we see a much stronger extratropical precipitation response to SST changes (Figure 6, third row). As with these other studies, our experiments produce overall subtropical drying and high-latitude moistening, but our results suggest that the direct effects of ozone and greenhouse gases play only a secondary role compared to the indirect SST effect.

[Figure 6 about here]

Why the indirect SST effect is so much stronger in our study than in DP09, P10, or K11 is not clear. We use decadally averaged SSTs taken from coupled model 20C3M and A1B scenarios. DP09 perform ensemble transient experiments with observed SSTs, but P10 and but K11both use multi-year averaged SSTs as we do, so it is unlikely that natural SST variability is confounding our results or the results of P10 or K11.

To understand the differing ozone responses in our work compared toP10, we refer to Figure 3 in Son et al. (2008). CM2.1 (the coupled model companion to AM2.1) has a weaker polar cap temperature response than CCSM3 (the coupled model companion to CAM3). Assuming the differences between prescribed ozone changes in the two studies are small, CM2.1 is less sensitive to ozone depletion than CCSM3, and by extension AM2.1 may be less sensitive than CAM3 as well. However, we note that data from the standard 24-level configuration of CM2.1 were examined in Son et al. (2008), while we use a 48-level version of AM2.1. We calculate that the SH lower stratosphere temperature response to the combined forcings is 30% stronger in our high-top configuration of AM2.1 than in the standard 24-level AM2.1 configuration. This increasing sensitivity with vertical resolution is expected (Karpechko et al. 2008), and may 'close the gap' in sensitivity somewhat between AM2.1 and CAM3.

Which of the many projections is more accurate remains to be seen (Perlwitz 2011). What this study demonstrates is that even among realistic models, with carefully prescribed ozone recovery and a well-resolved stratosphere, the halting or reversing of the poleward SH jet shift during the coming century is strongly model dependent.

Acknowledgements

We gratefully acknowledge the assistance of Junsu Kim. Allocation of computer time from the Center for High Performance Computing at the University of Utah is also gratefully acknowledged. This research was supported by the NSF-GK12 program, NSF grant ATM0532280, and NOAA grant OAR-OGP-2006-2000116.

References

Anderson JL, Balaji V, Broccoli AJ, Cooke WF, Delworth TL, Dixon KW, Donner LJ, Dunne KA, Freidenreich SM, Garner ST, Gudgel RG, Gordon CT, Held IM, Hemler RS, Horowitz LW, Klein SA, Knutson TR, Kushner PJ, Langenhost AR, Lau NC, Liang Z, Malyshev SL, Milly PCD, Nath MJ, Ploshay JJ, Ramaswamy V, Schwarzkopf MD, Shevliakova E, Sirutis JJ, Soden BJ, Stern WF, Thompson LA, Wilson RJ, Wittenberg AT, Wyman BL, Dev

GGAM (2004) The new GFDL global atmosphere and land model AM2-LM2: Evaluation with prescribed SST simulations. J Climate 17 (24):4641-4673

Arblaster JM, Meehl GA (2006) Contributions of external forcings to southern annular mode trends. J Climate 19 (12):2896-2905

Baldwin MP, Thompson DWJ (2009) A critical comparison of stratosphere–troposphere coupling indices. Q J Roy Meteor Soc 135 (644):1661-1672

Cionni I, Eyring V, Lamarque J-F, Randel WJ, Stevenson DS, Wu F, Bodeker GE, Shepherd TG, Shindell DT, Waugh DW (2011) Ozone database in support of CMIP5 simulations: results and corresponding radiative forcing. Atmos Chem Phys 11:10875–10933. doi:10.5194/acpd-11-10875-2011

Delworth TL, Broccoli AJ, Rosati A, Stouffer RJ, Balaji V, Beesley JA, Cooke WF, Dixon KW, Dunne J, Dunne KA, Durachta JW, Findell KL, Ginoux P, Gnanadesikan A, Gordon CT, Griffies SM, Gudgel R, Harrison MJ, Held IM, Hemler RS, Horowitz LW, Klein SA, Knutson TR, Kushner PJ, Langenhorst AR, Lee HC, Lin SJ, Lu J, Malyshev SL, Milly PCD, Ramaswamy V, Russell J, Schwarzkopf MD, Shevliakova E, Sirutis JJ, Spelman MJ, Stern WF, Winton M, Wittenberg AT, Wyman B, Zeng F, Zhang R (2006) GFDL's CM2 global coupled climate models. Part I: Formulation and simulation characteristics. J Climate 19 (5):643-674

Deser C, Phillips AS (2009) Atmospheric circulation trends, 1950-2000: the relative roles of sea surface temperature forcing and direct atmospheric radiative forcing. J Climate 22 (2):396-413

Fletcher CG, Hardiman SC, Kushner PJ, Cohen J (2009) The Dynamical Response to Snow Cover Perturbations in a Large Ensemble of Atmospheric GCM Integrations. J Climate 22 (5):1208-1222. doi:10.1175/2008JCLI2505.1

Gerber EP, Baldwin MP, Akiyoshi H, Austin J, Bekki S, Braesicke P, Butchart N, Chipperfield M, Dameris M, Dhomse S, Frith SM, Garcia RR, Garny H, Gettelman A, Hardiman SC, Karpechko A, Marchand M, Morgenstern O, Nielsen JE, Pawson S, Peter T, Plummer DA, Pyle JA, Rozanov E, Scinocca JF, Shepherd TG, Smale D (2009) Stratosphere-troposphere coupling and annular mode variability in chemistry-climate models. J Geophys Res 115:D00M06. doi:10.1029/2009JD013770

Gillet NP, Thompson DWJ (2003) Simulation of recent Southern Hemisphere climate change. Science 302 (5643):273-275

Hu Y, Fu Q (2007) Observed poleward expansion of the Hadley circulation since 1979. Atmos Chem Phys 7 (19):5229-5236

Hu Y, Zhou C, Liu J (2011) Observational evidence for poleward expansion of the Hadley circulation Adv Atmos Sci 28 (1):33-44. doi: 10.1007/s00376-010-0032-1

Johanson CM, Fu Q (2009) Hadley cell widening: model simulations versus observations. J Climate 22 (10):2713-2725

Kang SM, Polvani LM (2010) The interannual relationship between the latitude of the eddy-driven jet and the edge of the Hadley cell. 24 (2):563-568. doi:10.1175/2010JCLI4077.1

Kang SM, Polvani LM, Fyfe JC, Sigmond M (2011) Impact of polar ozone depletion on subtropical precipitation. Science 332:951-954. doi:10.1126/science.1202131

Karpechko AY, Gillett NP, Marshall GJ, Scaife AA (2008) Stratospheric influence on circulation changes in the Southern Hemisphere troposphere in coupled climate models. Geophys Res Lett 35 (20):L20806

Kidston J, Gerber EP (2010) Intermodel variability of the poleward shift of the austral jet stream in the CMIP3 integrations linked to biases in 20th century climatology. Geophys Res Lett 37 (9):L09708

Kidston J, Vallis GK (2010) Relationship between eddy-driven jet latitude and width. Geophys Res Lett 37 (21):L21809

Kushner PJ, Held IM, Delworth TL (2001) Southern Hemisphere atmospheric circulation response to global warming. J Climate 14 (10):2238-2249

Leith CE (1975) Climate Response and Fluctuation Dissipation. J Atmos Sci 32 (10):2022-2026

Lu J, Chen G, Frierson DMW (2010) The Position of the Midlatitude Storm Track and Eddy-Driven Westerlies in Aquaplanet AGCMs. J Atmos Sci 67 (12):3984-4000. doi:10.1175/2010JAS3477.1

Lu J, Deser C, Reichler T (2009) Cause of the widening of the tropical belt since 1958. Geophys Res Lett 36:L03803

Lu J, Vecchi GA, Reichler T (2007) Expansion of the Hadley cell under global warming. Geophys Res Lett 34 (6):L06805

McLandress C, Shepherd TG, Scinocca JF, Plummer DA, Sigmond M, Jonsson AI, Reader MC (2011) Separating the dynamical effects of climate change and ozone depletion: Part II. Southern Hemisphere troposphere. J Climate 24 (6):1850–1868. doi:10.1175/2010JCLI3958.1

Miller RL, Schmidt GA, Shindell DT (2006) Forced annular variations in the 20th century intergovernmental panel on climate change fourth assessment report models. J Geophys Res 111 (D18):D18101

Ming Y, Ramaswamy V (2009) Nonlinear climate and hydrological responses to aerosol effects. J Climate 22 (6):1329-1339. doi:10.1175/2008JCLI2362.1

Nyquist H (1928) Thermal Agitation of Electric Charge in Conductors. Physical Review 32 (1):110

Perlwitz J, Pawson S, Fogt RL, Nielsen JE, Neff WD (2008) Impact of stratospheric ozone hole recovery on antarctic climate. Geophys Res Lett 35 (8). doi:10.1029/2008GL033317

Perlwitz J (2011) Atmospheric Science: Tug of war on the jet stream. Nature Clim Change 1 (1):29-31

Polvani LM, Kushner PJ (2002) Tropospheric response to stratospheric perturbations in a relatively simple general circulation model. Geophys Res Lett 29 (7):doi: 10.129/2001GL014284

Polvani LM, Previdi M, Deser C (2011) Large cancellation, due to ozone recovery, of future Southern Hemisphere atmospheric circulation trends. Geophys Res Lett 38 (4):L04707

Polvani LM, Waugh DW, Correa GJP, Son S-W (2010) Stratospheric ozone depletion: the main driver of 20th century atmospheric circulation changes in the Southern Hemisphere. J Climate 24:795-812. doi: 10.1175/2010JCLI3772.1

Reichler T (2009) Changes in the Atmospheric Circulation as Indicator of Climate Change. In: Letcher TM (ed) Climate Change: Observed impacts on Planet Earth. Elsevier,

Rosenlof KH (2002) Transport changes inferred from HALOE water and methane measurements. J Meteor Soc Japan 80 (4B):831-848

Rutz J (2010) Recent shifts in the general circulation: Causation, seasonality, and implications. M.S. Thesis, University of Utah, Salt Lake City

Seidel DJ, Fu Q, Randel WJ, Reichler TJ (2008) Widening of the tropical belt in a changing climate. Nature Geosci 1 (1):21-24

Seidel DJ, Randel WJ (2007) Recent widening of the tropical belt: Evidence from tropopause observations. J Geophys Res 112 (D20):D20113

Son S-W, Polvani LM, Waugh DW, Akiyoshi H, Garcia R, Kinnison D, Pawson S, Rozanov E, Shepherd TG, Shibata K (2008) The impact of stratospheric ozone recovery on the Southern Hemisphere westerly jet. Science 320 (5882):1486-1489

Son S-W, Polvani LM, Waugh DW, Birner T, Akiyoshi H, Garcia RR, Gettelman A, Plummer DA, Rozanov E (2009a) The impact of stratospheric ozone recovery on tropopause height trends. J Climate 22 (2):429-445

Son S-W, Tandon NF, Polvani LM, Waugh DW (2009b) Ozone hole and Southern Hemisphere climate change. Geophys Res Lett 36:-. doi:10.1029/2009GL038671

Son SW, Gerber EP, Perlwitz J, Polvani LM, Gillett NP, Seo KH, Eyring V, Shepherd TG, Waugh D, Akiyoshi H, Austin J, Baumgaertner A, Bekki S, Braesicke P, Brühl C, Butchart N, Chipperfield MP, Cugnet D, Dameris M, Dhomse S, Frith S, Garny H, Garcia R, Hardiman SC, Jöckel P, Lamarque JF, Mancini E, Marchand M, Michou M, Nakamura T, Morgenstern O, Pitari G, Plummer DA, Pyle J, Rozanov E, Scinocca JF, Shibata K, Smale D, Teyssèdre H, Tian W, Yamashita Y (2010) Impact of stratospheric ozone on Southern Hemisphere circulation change: A multimodel assessment. J Geophys Res 115:D00M07

Staten PW, Reichler T, Lu J (2010) Understanding the direct and indirect circulation response to radiative forcings. Paper presented at the AGU Fall Meeting, San Francisco, CA, USA, 13-17 December. Available online at http://inscc.utah.edu/~pstaten/talks/Staten_2010_AGU_A33A-0149.pdf

Thompson DWJ, Wallace JM (2000) Annular modes in the extratropical circulation. Part I: Month-to-month variability. J Climate 13 (5):1000-1016

Zhou YP, Xu K-M, Sud YC, Betts AK (2011) Recent trends of the tropical hydrological cycle inferred from Global Precipitation Climatology Project and International Satellite Cloud Climatology Project data. J Geophys Res 116 (D9):D09101

Figure Captions

Fig 1. Zonal mean (a) column-integrated ozone (in Dobson units) and (b, c) sea surface temperature forcings (in °C; negative contours dashed) used in this study, by season and latitude. Black solid and dashed contours show control climatology, while shading shows the change between the time periods shown.

Fig 2. Latitude-height cross-sections of reference temperature climatology for the simulations indicated at the left and change between the time periods shown at the top during December-January-February. Gray hatching represents changes that are not significant at the 5% level.

Fig 3. As for Figure 2 but for zonal wind (in m/s; negative contours dashed). Contours are spaced 10 ms^{-1} apart, starting at 5 ms^{-1}.

Fig 4. The seasonality of shifts in the zonal mean circulation indicators listed at the left and described in section 2. Shifts are shown in degrees latitude, except for the annular mode (bottom row), in which case values reflect normalized changes in the annular mode indices (in standard deviations). Note the different scale used for the Ferrel cell edge (third row). The color of each curve denotes the type of forcing, as shown at the bottom. Column headings indicate time periods for which differences are calculated. Thick lines highlight statistically significant shifts at the 5% level. Thin gray lines indicate the linear sum of the changes for each type of forcing. Each panel is divided into two parts, with the upper half showing NH changes, and the lower half showing SH changes. Numbers in the first column indicate the pre-industrial annual mean latitudes for each feature.

Fig 5. As in Figure 4, but for the hydrological indicators listed at the left.

Fig 6. Changes in December-January-February precipitation (in mm/day), for the time periods shown at the top, and the forcing type shown at the left. The zonal mean changes are depicted to the right of each map (also in mm/day), with the global mean change listed next to each latitudinal profile.

Fig S1. As with Figure 2 but for June-July-August.

Fig S2. As with Figure 3 but for June-July-August.

Fig S3. Left column as with Figure 2 and right column as with Figure 3, but for changes between present-day and the year 2100.

Table 1 Simulations performed in this study, grouped by the time period examined

group	name	forcings O_3	forcings CO_2	forcings SST	description
2000-1870	control	-	-	-	pre-industrial
	O_3	✓*	-	-	depleted O_3
	CO_2	-	✓	-	present-day CO_2
	SST	-	-	✓	present-day SSTs
	all	✓	✓	✓	present-day
2050-2000	control	✓	✓	✓	present-day
	O_3	-**	✓	✓	recovered O_3
	CO_2	✓	✓✓	✓	2050 CO_2
	SST	✓	✓	✓✓	2050 SST
	all	-	✓✓	✓✓	2050 conditions
2100-2000	O_3 control	✓	✓	✓	present-day
	O_3	-	✓	✓	recovered O_3
	CO_2 control	-	✓	-	present-day CO_2 only
	CO_2	-	✓✓✓	-	2100 CO_2 only
	SST control	-	-	✓	present-day SSTs only
	SST	-	-	✓✓✓	2100 SSTs only
	all control	✓	✓	✓	present-day
	all	-	✓✓✓	✓✓✓	year-2100

* '-', ✓, ✓✓, and ✓✓✓ signify that a given forcing is set at pre-industrial, present-day, 2050, and 2100 levels, respectively.

** '-' is used for pre-industrial and recovered ozone levels, since we use historic rather than projected levels for ozone recovery.

UU IR Author Manuscript

Table 2 Annual mean shifts (in degrees latitude*) in the zonal mean circulation features NH and SH values are paired, with NH values appearing above SH values. '2000', '2050', and '2100' are used here as described in the text.

	O3			CO2			SST			All		
	2000	2050	2100	2000	2050	2100	2000	2050	2100	2000	2050	2100
Hadley cell edge	(-0.01)**	(0.02)	(0.02)	0.08	0.07	0.13	0.07	0.43	0.68	0.18	0.50	0.74
	-0.07	0.06	0.06	-0.12	-0.10	-0.21	-0.32	-0.16	-0.61	-0.57	-0.17	-0.78
surface U zero crossing	(-0.01)	(0.02)	(0.02)	0.17	0.05	0.19	0.39	0.57	0.60	0.56	0.70	0.79
	-0.12	0.11	0.11	-0.23	-0.14	-0.31	-0.56	-0.26	-0.73	-0.98	-0.28	-0.98
Ferrel cell edge	-0.18	0.14	0.14	0.30	(0.06)	0.40	0.70	1.54	2.37	1.01	2.06	3.27
	-0.27	0.27	0.27	-0.39	-0.25	-0.49	-0.70	-0.36	-1.15	-1.52	-0.34	-1.25
annular mode*	(-0.01)	(-0.01)	(-0.01)	0.09	(0.03)	0.09	0.34	0.26	0.48	0.47	0.33	0.57
	0.20	-0.21	-0.21	0.30	0.20	0.39	0.75	0.42	1.02	1.40	0.42	1.17
P-E zero crossing	0.07	-0.08	-0.08	0.31	0.18	0.46	1.11	0.81	1.16	1.53	0.92	1.55
	-0.23	0.21	0.21	-0.44	-0.36	-0.58	-1.10	-1.04	-1.67	-1.92	-1.06	-2.16
precipitation maximum	(0.01)	-0.07	-0.07	(0.00)	(0.00)	(-0.01)	0.30	0.62	0.60	0.35	0.60	0.61
	-0.07	0.05	0.05	-0.11	-0.06	-0.13	-0.53	-0.44	-0.73	-0.74	-0.45	-0.84

* Annular mode shifts are in standard deviations

** Values in parenthesis are not statistically significant at a 5% level.

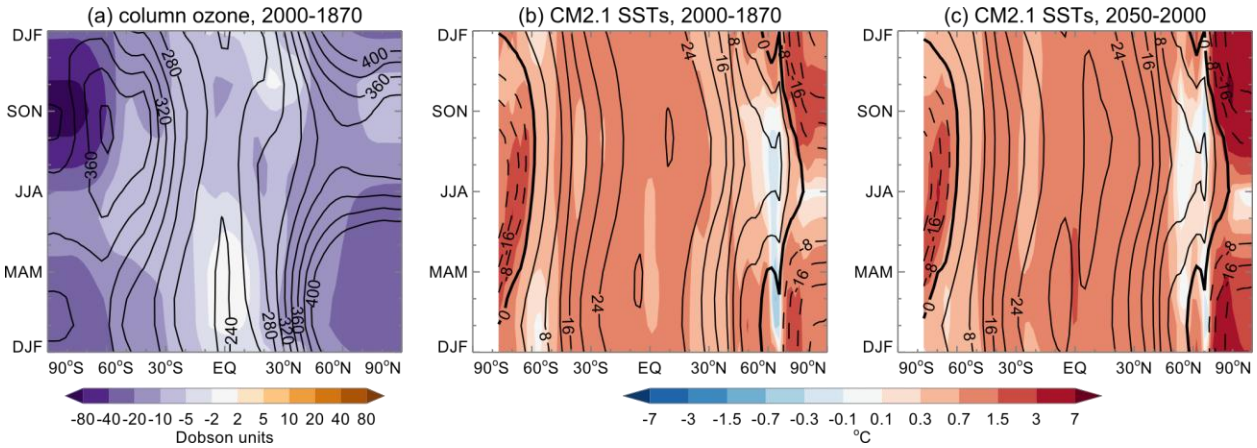

Fig 1. Zonal mean (a) column-integrated ozone (in Dobson units) and (b, c) sea surface temperature forcings (in °C; negative contours dashed) used in this study, by season and latitude. Black solid and dashed contours show control climatology, while shading shows the change between the time periods shown.

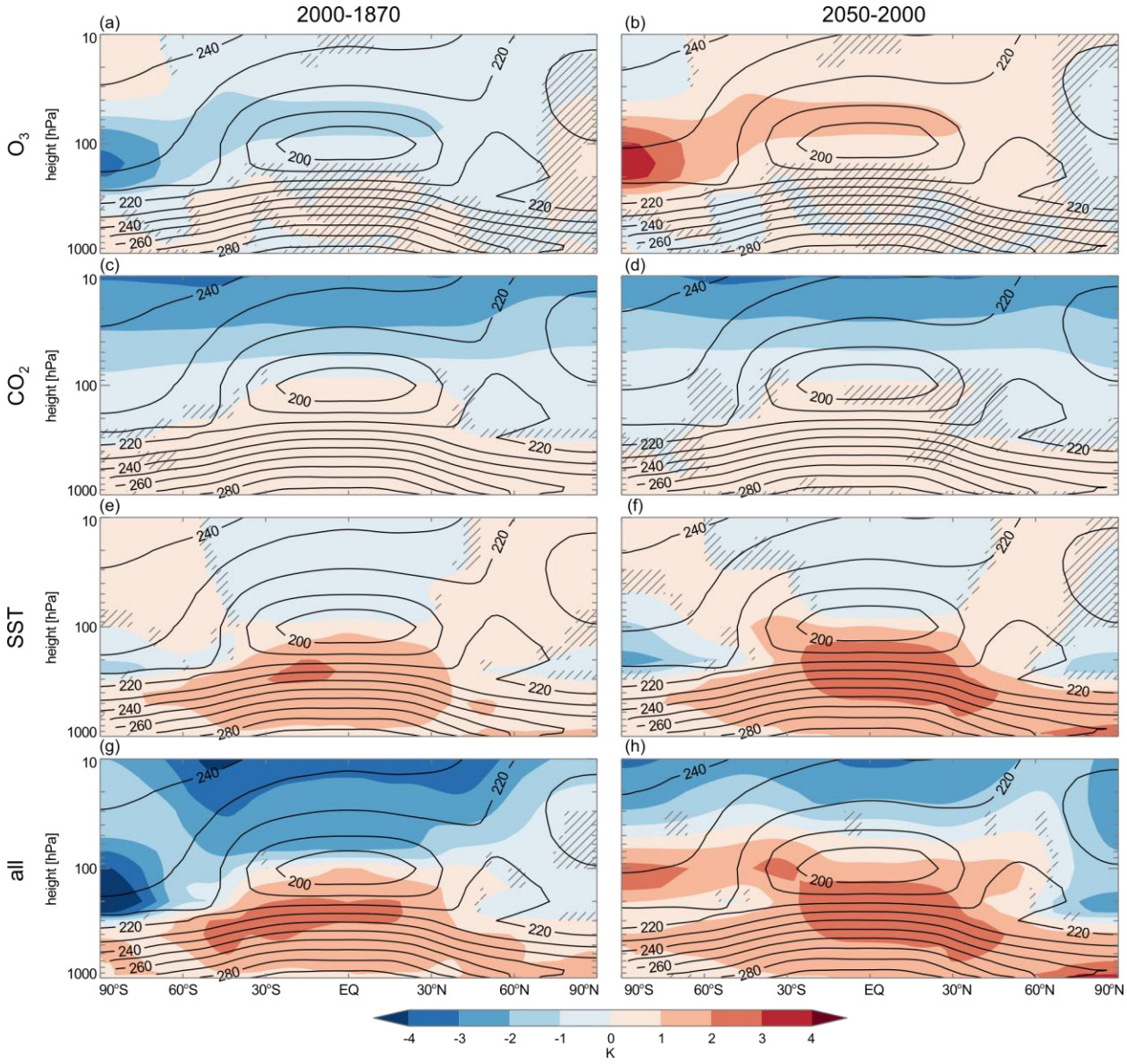

Fig 2. Latitude-height cross-sections of reference temperature climatology for the simulations indicated at the left and change between the time periods shown at the top during December-January-February. Gray hatching represents changes that are not significant at the 5% level.

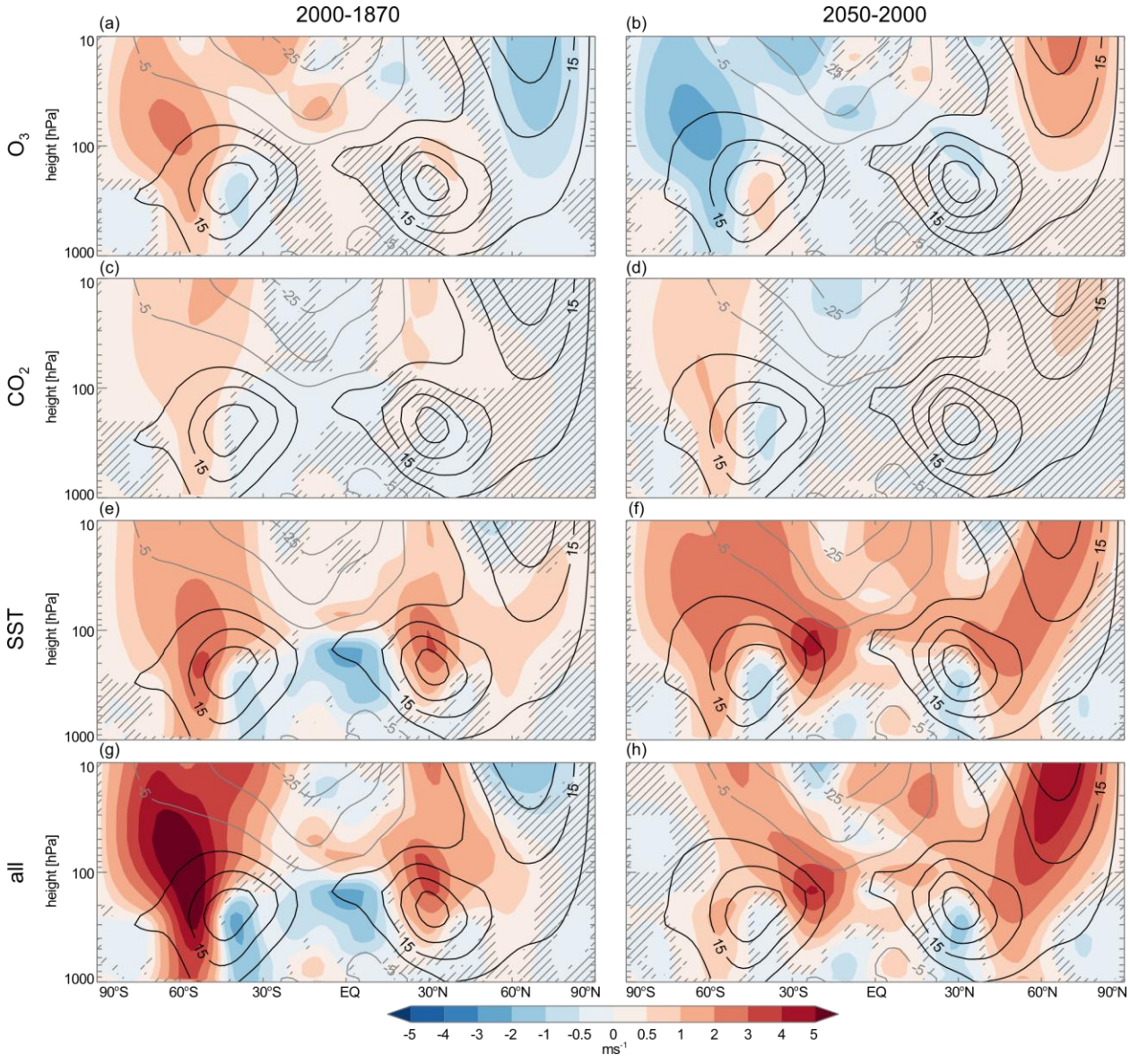

Fig 3. As for Figure 2 but for zonal wind (in m/s; negative contours dashed). Contours are spaced 10 ms^{-1} apart, starting at 5 ms^{-1}.

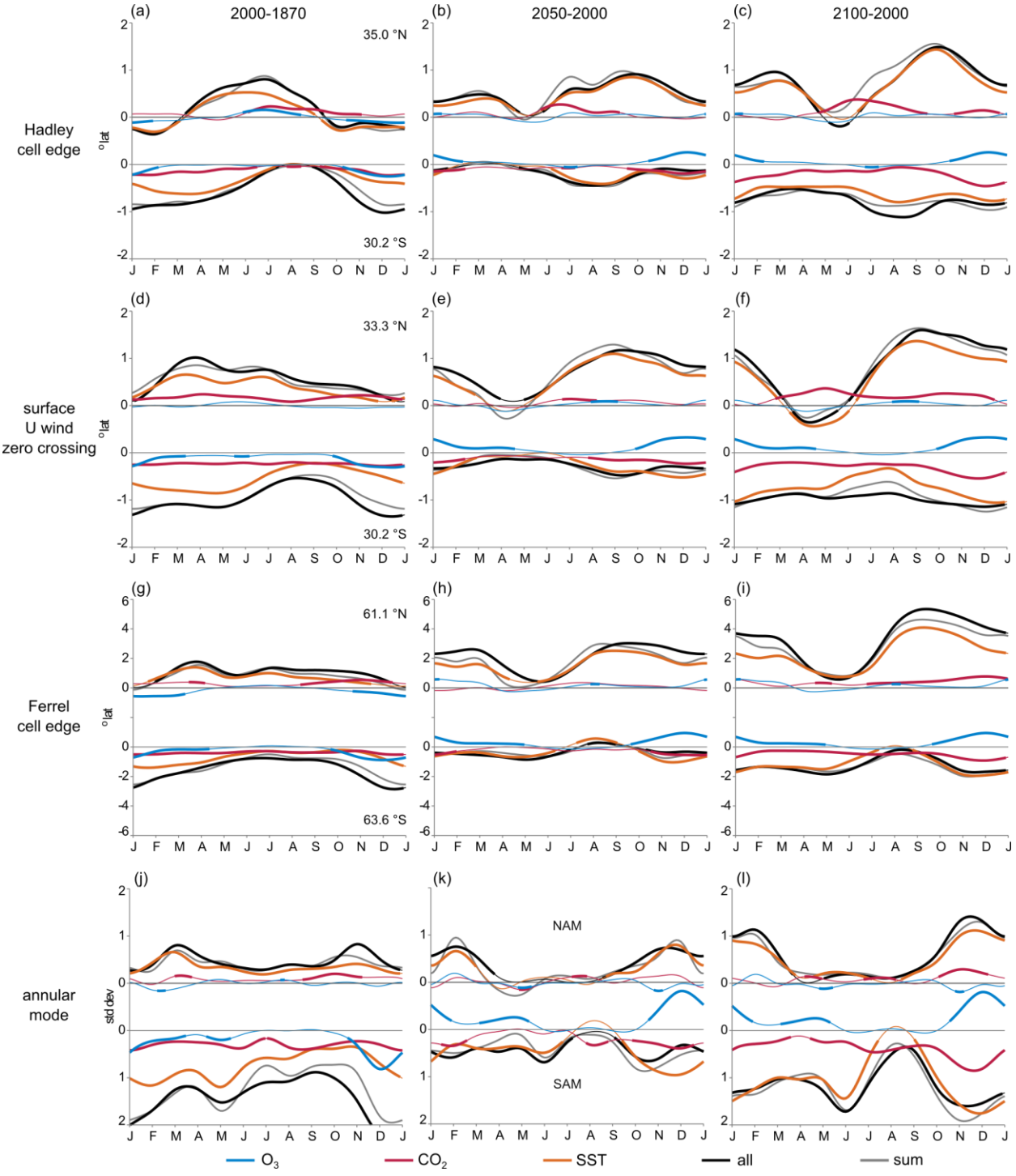

UU IR Author Manuscript

Fig 4. The seasonality of shifts in the zonal mean circulation indicators listed at the left and described in section 2. Shifts are shown in degrees latitude, except for the annular mode (bottom row), in which case values reflect normalized changes in the annular mode indices (in standard deviations). Note the different scale used for the Ferrel cell edge (third row). The color of each curve denotes the type of forcing, as shown at the bottom. Column headings indicate time periods for which differences are calculated. Thick lines highlight statistically significant shifts at the 5% level. Thin gray lines indicate the linear sum of the changes for each type of forcing. Each panel is divided into two parts, with the upper half showing NH changes, and the lower half showing SH changes. Numbers in the first column indicate the pre-industrial annual mean latitudes for each feature.

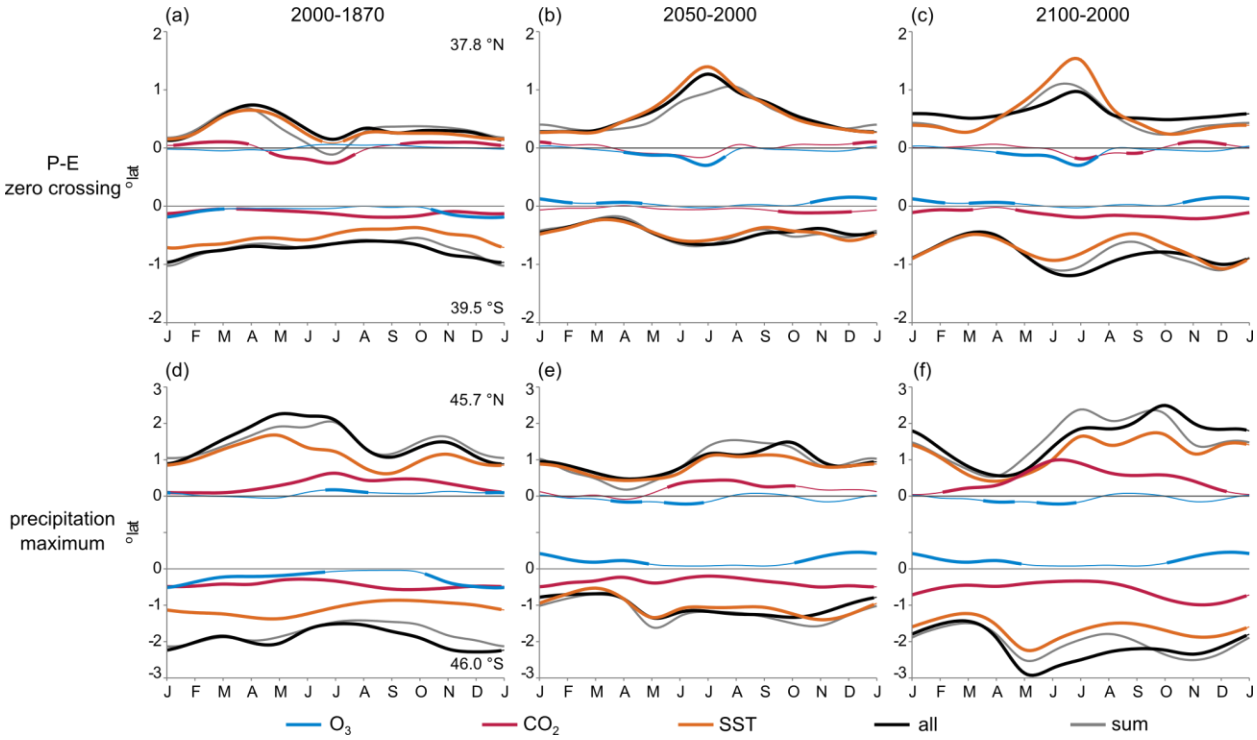

Fig 5. As in Figure 4, but for the hydrological indicators listed at the left.

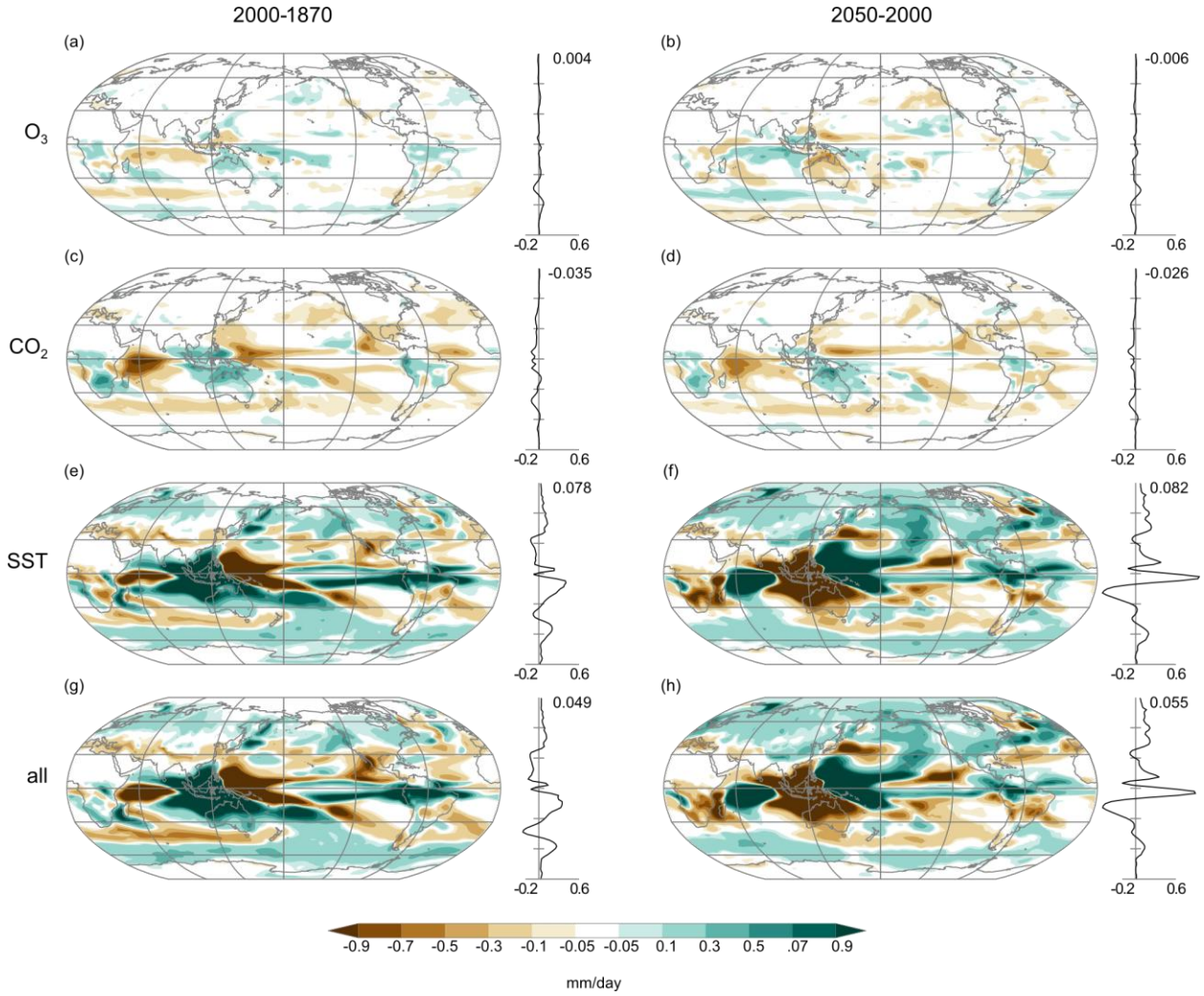

Fig 6. Changes in December-January-February precipitation (in mm/day), for the time periods shown at the top, and the forcing type shown at the left. The zonal mean changes are depicted to the right of each map (also in mm/day), with the global mean change listed next to each latitudinal profile.

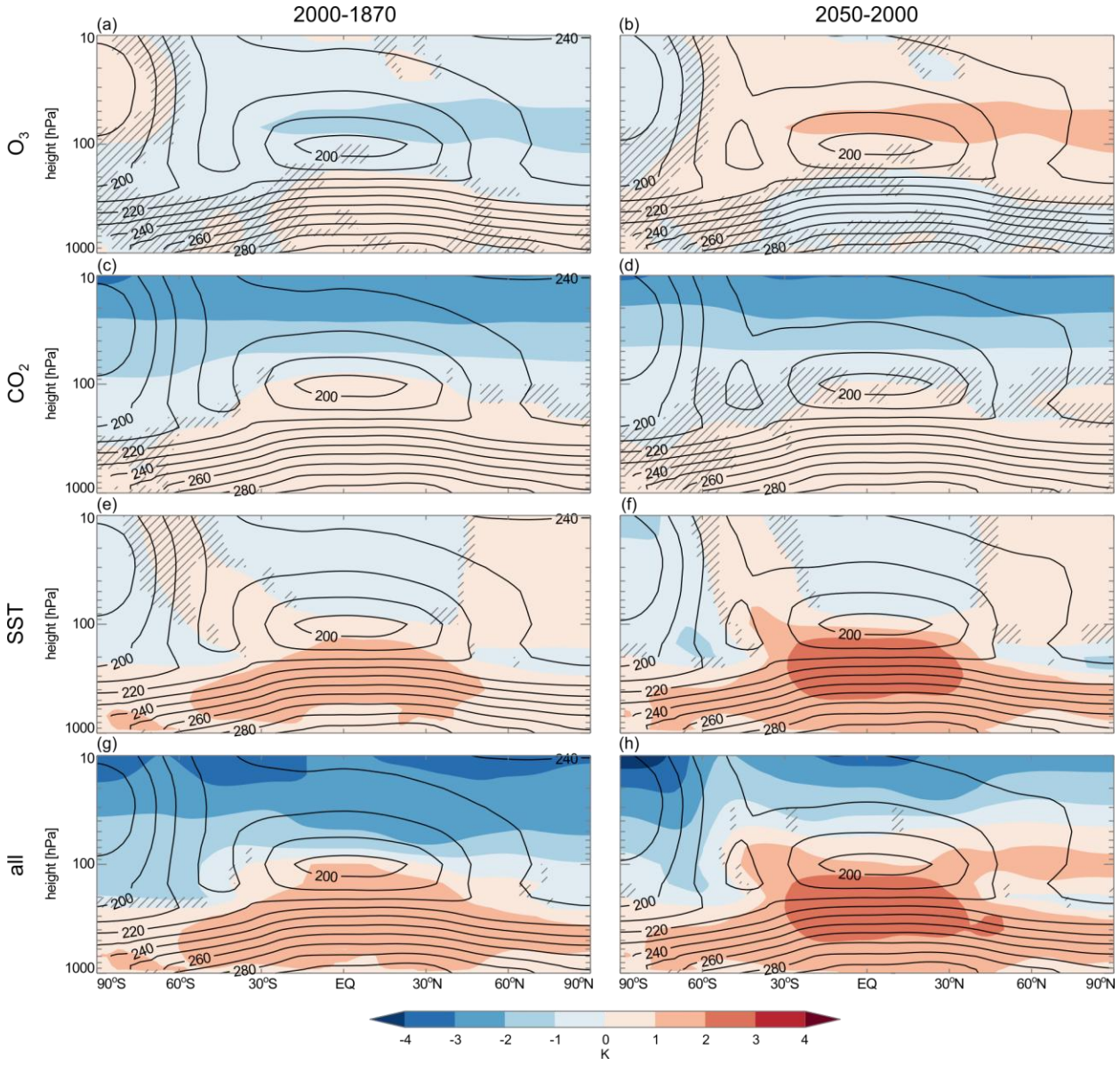

Fig S1. As with Figure 2 but for June-July-August.

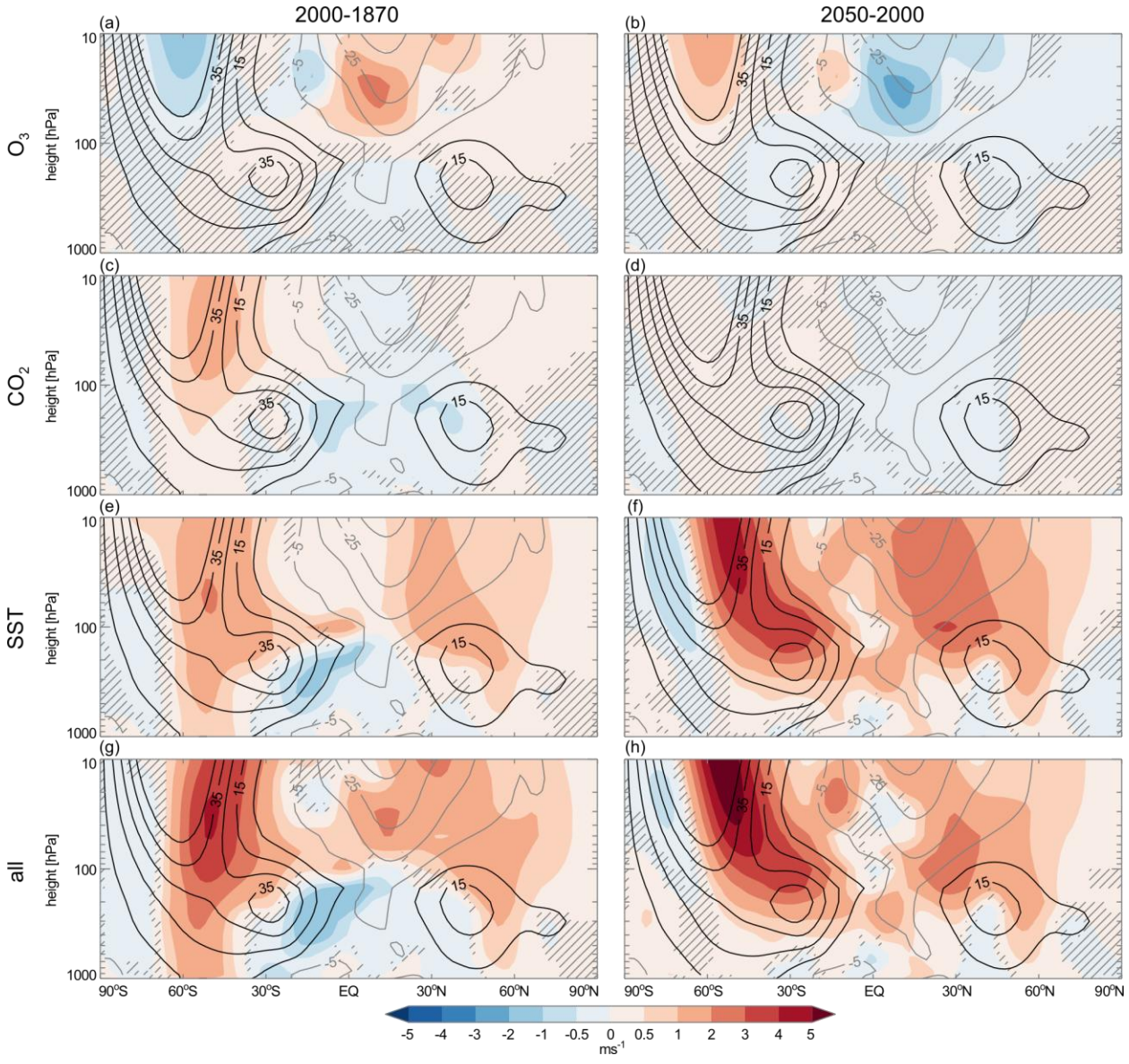

Fig S2. As with Figure 3 but for June-July-August.

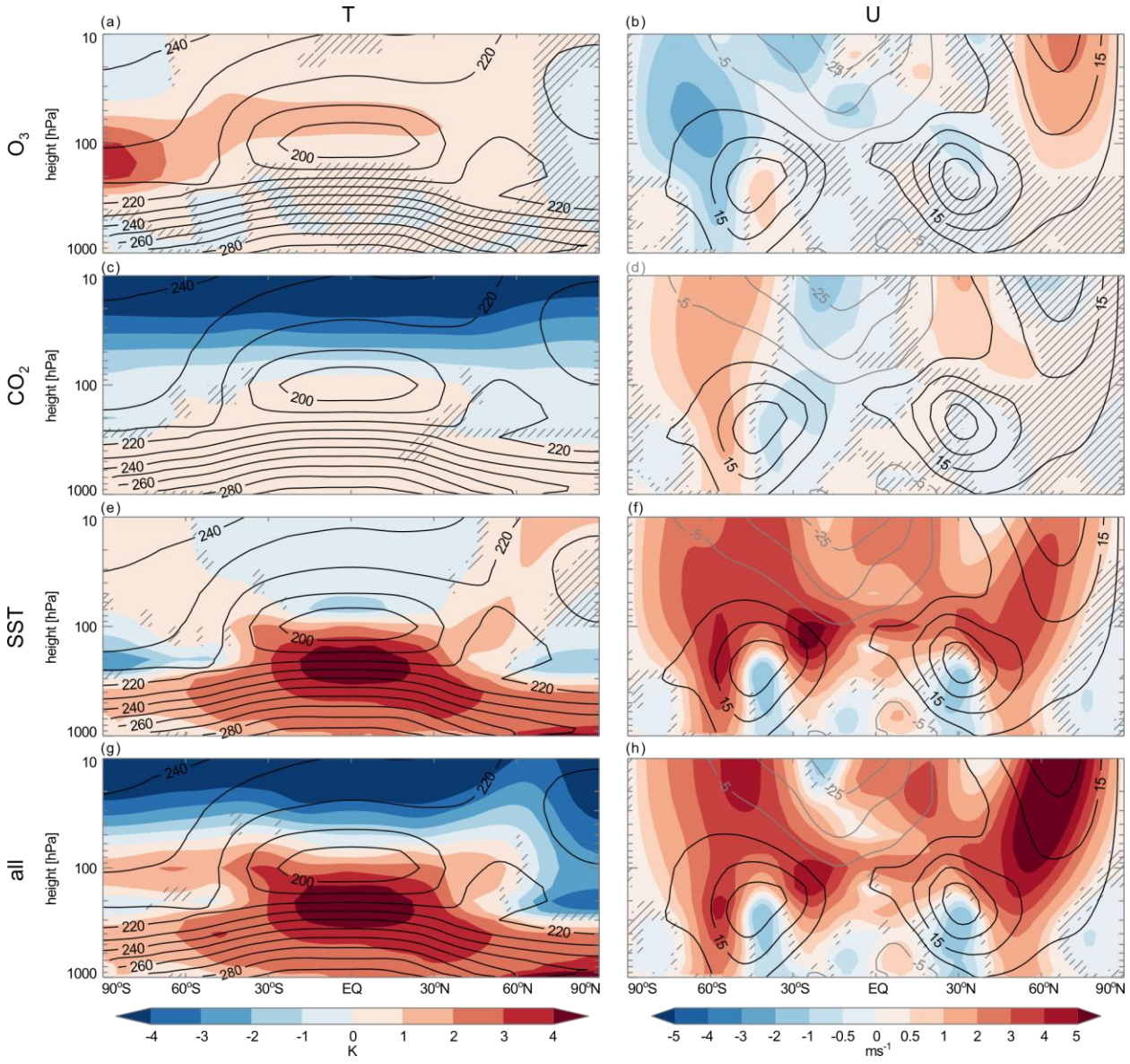

Fig S3. Left column as with Figure 2 and right column as with Figure 3, but for changes between present-day and the year 2100.